NUMERICAL SIMULATIONS ON THE ROTATING FLOW OF WRAPPED WIRED HPLWR FUEL ASSEMBLY

Attila Kissa[1], Eckart Laurien[2], Attila Aszódia[1], Yu Zhu[2]
[1] Institute of Nuclear Techniques (NTI), Budapest University of Technology and Economics,
E-mail: kissa@reak.bme.hu
[2] Institute for Nuclear Technology and Energy Systems (IKE), University of Stuttgart,
E-mail: Laurien@ike.uni-stuttgart.de

Abstract

Three dimensional computational-fluid-dynamics simulations are performed for the fluid flow within a 40 rod fuel bundle in a square arrangement with a central moderator channel. To ensure spacing between the rods the design of the bundle uses thin wires wrapped counter-clockwise around each rod. This geometry is presently investigated in the framework of the European High-Performance Light-Water Reactor (HPLWR), which operates at supercritical pressure of 25 MPa. A section with one revolution located in the evaporator region of the HPLWR core is investigated using hydraulic (to ensure fully developed flow inlet boundary conditions and reference for heated cases) and thermal-hydraulic boundary conditions. The geometry of wrapped wires gives rise to additional mixing and a circulating or 'sweeping' flow near the outer and inner regions of the fuel element next to the wall of the so called fuel assembly and moderator box. Some interesting flow features associated with the complex three-dimensional flow with significant transverse velocity components are visualized as the first evaluated result of this diversified investigation.

1. Introduction

The flow and heat transport in nuclear fuel rod assemblies depends on the conditions at the assembly inlet, the surface temperature and heat flux of the fuel rods, the coolant properties and the geometry of the assembly. In some rector concepts, e.g. the European High-Performance Light-Water Reactor (HPLWR) [1,2], wires are wrapped around each fuel rod to guarantee proper spacing and simultaneously enhance the flow mixing within a fuel element. The geometry of such assemblies is rather complex and the effect of the wires on the mass, momentum and energy transfer between its various sub-channels is not fully understood. Therefore both experimental [3] as well as numerical sub-channel analyses [4,5] have been performed. To investigate such flows in detail various numerical investigations [6,7,8] are underway using the method of Computational Fluid Dynamics (CFD).

In the present study the 40-rod bundle of the HPLWR with an outer fuel element box and an inner moderator channel, see [1], is investigated with the CFD-code CFX-11. A thin wire is wrapped counter-clockwise around each rod to provide both spacing and improve thermal mixing within the fuel element. The length of one revolution (wire pitch) is 200 mm. In a previous study [9] only a quarter of the fuel element was investigated using the approximate "opening" boundary conditions (in "CFX" notation) at the cutting surfaces due to the lack of exact symmetry conditions. It was found, however, that in spite of good convergence of the iteration some expected flow symmetries in the results could not be reproduced with satisfactory accuracy. Therefore, in the present paper, the entire bundle without any cutting surfaces is computed, increasing the necessary numerical effort at least fourfold. The project is performed within the European High-Performance Computing program, HPC-Europe 2, using up to 32 processors on a 4-16 parallel computer. The aim of this study is to understand and model the transport of mass, momentum and heat between neighbouring sub-channels induced by the wrapped wire spacers and the increased flow resistance of the sub-channels.

2. Geometry and the Mathematical / Physical Models

A full HPLWR fuel assembly model with whole perimeter is investigated in this paper. The integration domain is a section with one counter-clockwise revolution of the wrapped wire spacer (which reference length is 200 mm) located in different positions of the evaporator region of the HPLWR core. The schematics of the fuel assembly structure and its dimensions can be seen on left and right side of Fig. 1 respectively. The assembly is designed with a pitch of 9.44 mm and rod diameters of 8 mm.

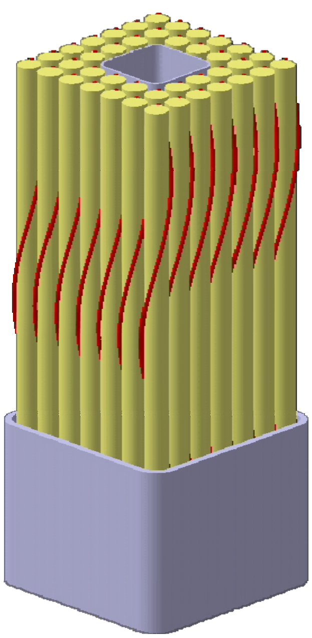

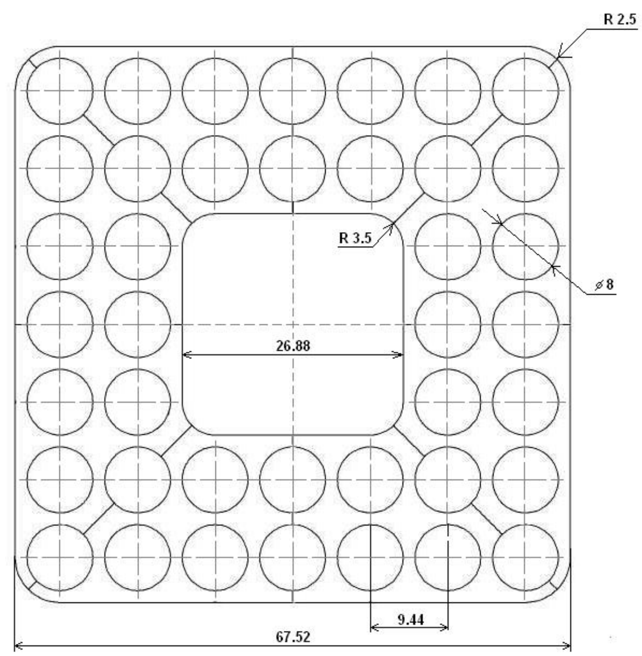

Figure 1. The schematics of the fuel assembly structure (left) and its dimensions (right, without indicating the wrapped wires).

The geometry of the fuel assembly, the Descartes coordinate system (x y z), the boundary regions and the simplified cross section of the wires can be seen on Fig. 2. The quasi-diameter of the wires is 1.34 mm which means there is a 0.1 mm distance between the fuel rods or other walls and the wires. This distance is in order to easier meshing procedure.

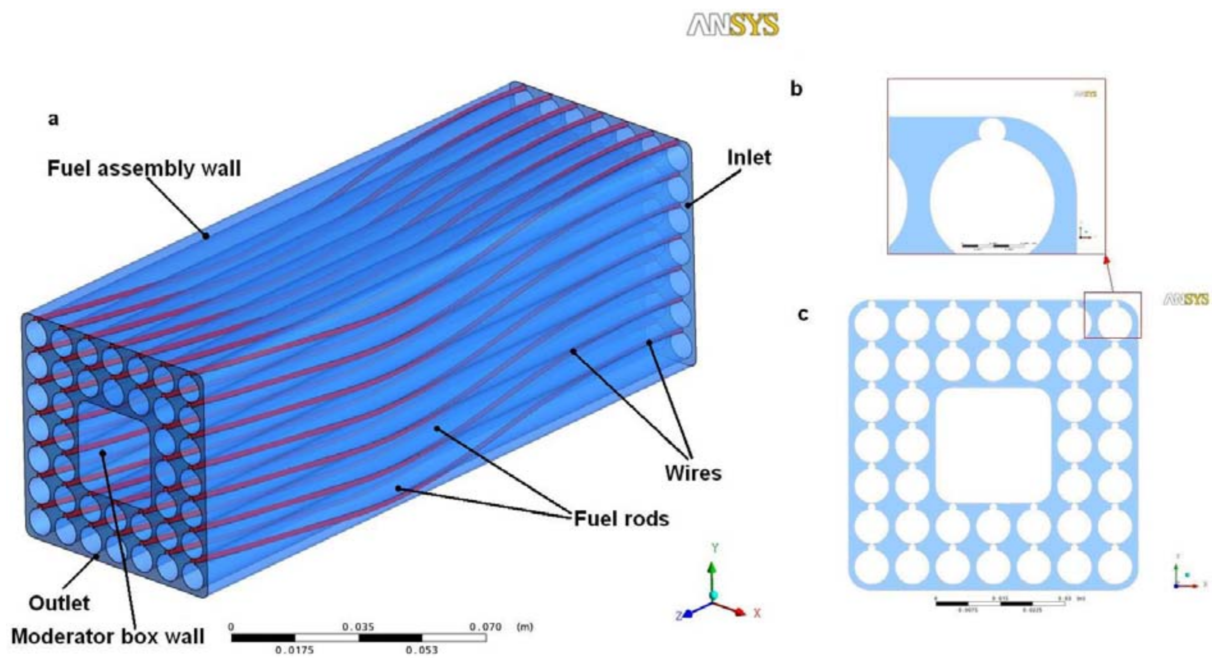

Figure 2. a., The geometry, boundary regions and coordinate system (x y z) of the model b., the simplified cross section of the wires c., the Inflow region of the model.

Six boundary regions are modelled: the inflow and outflow regions denoted as **Inlet** and **Outlet**, the wall of fuel rods and wrapped wires denoted as **Fuel rods** and **Wires**, the outer wall of moderator box and the inner wall of fuel assembly box denoted as **Moderator box wall** and **Fuel assembly wall**.

The position of seeding points of the wrapped wires are identical at each fuel rod on the Inlet boundary region as it can be seen on Fig. 2 a. The rotation direction of the wires is counter-clockwise from the top view (see Fig. 2 a).

Investigating the distributions of material properties (see Fig. 3), the heat flux and bulk fluid temperature calculated in a previous study [5] (see Fig 4) three thermal hydraulically interested regions can be identified in the evaporator pass:

- 1st region where maximal axial gradient of heat flux and bulk temperature occur from 0 m to 0.6 m – 3 revolutions (600 mm), the material properties alter moderately, the heat capacity has a relatively low value, the density, kinematic viscosity and heat conductivity are relatively high (this region is denoted as 1stR);

- 2nd region where the steep change in material properties occurs due to the pseudo-critical transition, this region is located from 1.4 m to 2 m – 3 revolutions, the bulk temperature stagnates due to high isobaric specific heat, the heat flux strongly decreases in the upstream direction (this region is denoted as 2ndR);

- 3rd region where the material properties are almost constant and relatively low, the bulk temperature slightly increases, the heat flux strongly decreases in the downstream direction, this region is located from 3.4 m to 4 m – 3 revolutions (this region is denoted as 3rdR).

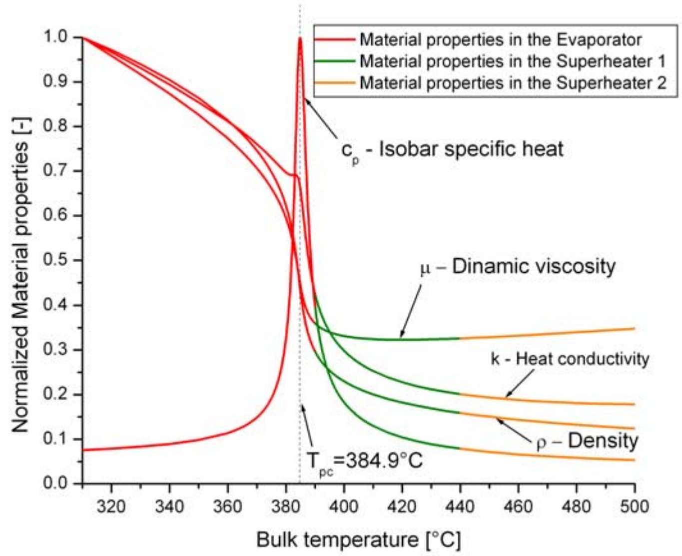

Figure 3. The distribution of material properties at 250 bar in the three pass of HPLWR core.

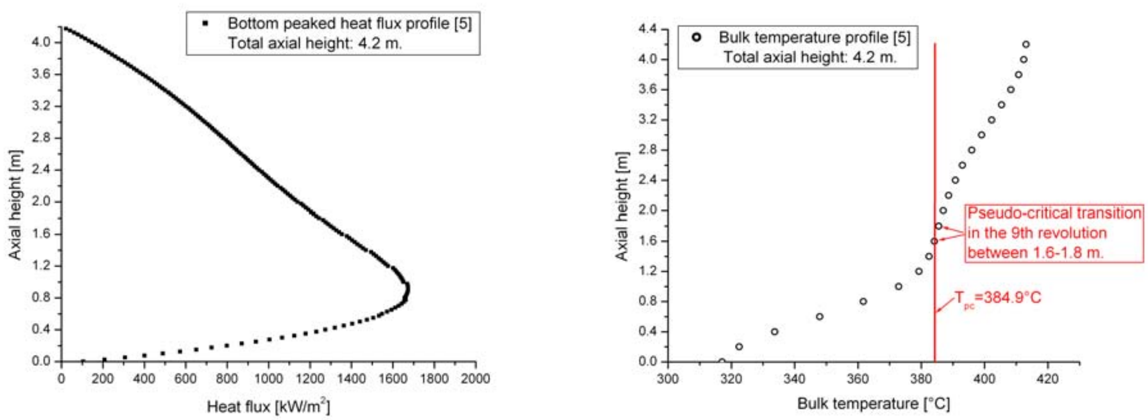

Figure 4. The distribution of heat flux (left) and bulk fluid temperature (right) in the evaporator along the axial height.

A large number of computation cases have been performed in two main groups: one hydraulic computation group (denoted as HDR-G) and one thermal hydraulic computation group (denoted as TH-G). The different cases can be seen in Table I.

Table I. The different computational cases (Italic style indicates cases for mesh sensitivity).

Group	Name of the case	Number of nodes	Mesh scale	Inflow/Outflow BC	Axial position
HDR-G Unheated	*Msh-1 (Coarse)*	222,000	1 to Msh-1	Translational periodic	0-0.2 m
	Msh-2	443,000	2 to Msh-1	Translational periodic	0-0.2 m
	Msh-3	600,000	3 to Msh-1	Translational periodic	0-0.2 m
	Msh-4 (Middle)	809,000	4 to Msh-1	Translational periodic	0-0.2 m
	Msh-5	1,100,000	5 to Msh-1	Translational periodic	0-0.2 m
	Msh-6	1,810,000	9 to Msh-1	Translational periodic	0-0.2 m
	Msh-7 (Fine)	3,082,000	16 to Msh-1	Translational periodic	0-0.2 m
	1stR	1,671,793	-	Translational periodic	0-0.2 m
	2ndR	1,671,793	-	Translational periodic	1.4-1.6 m
	3rdR	1,671,793	-	Translational periodic	3.4-3.6 m
TH-G Heated	*2ndR2 n 369k*	369,000	1 to n 369k	Inlet/Outlet	1.6-1.8 m
	2ndR2 n 563k	563,000	2 to n 369k	Inlet/Outlet	1.6-1.8 m
	2ndR2 n 907k	907,000	3 to n 369k	Inlet/Outlet	1.6-1.8 m
	1stR1	1,671,793	-	Inlet/Outlet	0-0.2 m
	1stR2	1,671,793	-	Inlet/Outlet	0.2-0.4 m
	1stR2 qw constant	1,671,793	-	Inlet/Outlet	0.2-0.4 m
	1stR2 qw rad	1,671,793	-	Inlet/Outlet	0.2-0.4 m
	1stR3	1,671,793	-	Inlet/Outlet	0.4-0.6 m
	2ndR1	1,671,793	-	Inlet/Outlet	1.4-1.6 m
	2ndR2	1,671,793	5 to n 369k	Inlet/Outlet	1.6-1.8 m
	2ndR2 qw constant	1,671,793	-	Inlet/Outlet	1.6-1.8 m
	2ndR2 qw rad	1,671,793	-	Inlet/Outlet	1.6-1.8 m
	2ndR3	1,671,793	-	Inlet/Outlet	1.8-2 m
	3rdR1	1,671,793	-	Inlet/Outlet	3.4-3.6 m
	3rdR2	1,671,793	-	Inlet/Outlet	3.6-3.8 m
	3rdR2 qw constant	1,671,793	-	Inlet/Outlet	3.6-3.8 m
	3rdR2 qw rad	1,671,793	-	Inlet/Outlet	3.6-3.8 m
	3rdR3	1,671,793	-	Inlet/Outlet	3.8-4 m

Firstly one hydraulic case has been calculated in HDR-G group to investigate the mesh sensitivity of the hydraulic result using 7 different global mesh densities for the unstructured tetrahedral mesh (from Msh-1 to 7). After the selection of global mesh density, three hydraulic cases (1stR, 2ndR and 3rdR) have been performed in HDR-G group to generate fully developed inflow turbulence and velocity boundary conditions for the thermal hydraulic cases and to serve as a reference unheated case to each interested thermal region. Then three different thermal hydraulic cases have been performed for each thermally interested region into three sequential revolutions using corresponding axial heat flux distribution (see in Fig. 4). All three middle cases of thermally interested regions

(1stR2, 2ndR2, 3rdR2) have also been investigated with 909.572 kW/m2 constant heat flux (denoted as …R2 qw constant) and additional axial + radial heat flux distributions (denoted as …R2 qw rad). The numbering of sub-channels, fuel rods, gaps (bounding surfaces between two neighbouring sub-channels) and the radial heat flux factors can be seen in Fig. 5. The radial heat flux factor means that each row has its own multiplication factor to the axial heat flux distribution to represent a linear power gradient from the last row to the first row of fuel rods.

Reynolds stress turbulence models (RSM) have been used for the above mentioned cases to consider the turbulence anisotropy proposed by the previous study [10]. The RSM or second moment closure turbulence models use six independent equations to model the six tags of the Reynolds stress tensor. The RSM models capable to predict the strong anisotropic features of the turbulent flow contrast to the so called first order closure or eddy viscosity models which use generally two equations to model turbulent flows. The RSM SSG was used for the hydraulic mesh sensitivity study (from Msh-1 to Msh-7) in order to decrease the computational needs. After the selection of global mesh density the RSM-ω model was used instead of RSM SSG for the further cases. The well known "scalable wall function" model has been used to model the near wall region (Fig. 8 shows the appropriateness of RSM- ω with wall function for heat transfer).

250 bar reference pressure, -9.81 k gravity vector and proper inflow temperature (see Fig. 4) have been set for all cases. Different boundary conditions have been applied for the hydraulic and thermal hydraulic cases. The main difference between HDR-G and TH-G cases is the applied inflow-outflow boundary condition. Translational periodic boundary condition with 3.22 kg/s mass flow rate has been used for the unheated hydraulic cases which mean that the inflow and outflow boundary regions were connected by identical velocity and turbulent fields. This boundary condition produce fully developed hydraulic fields on the inflow-outflow regions but does not allow flow of altering material properties going through. 1stR, 2ndR and 3rdR cases have been used to generate fully developed velocity and turbulent fields for the Inlet boundary condition of thermal hydraulic cases 1stR1, 2ndR1 and 3rdR1. So fully developed hydraulic (pressure, velocity) and turbulence profiles (turbulent kinetic energy, turbulent eddy dissipation and the six Reynolds stress components) have been applied on the inflow and outflow regions as boundary profiles for the thermal hydraulic cases. Proper outlet relative pressure [5] and heat flux distribution of the fuel rod surfaces (using the distribution which can be seen on Fig. 4) have been set for each thermal case. The surfaces of wrapped wires, moderator and fuel assembly box walls have been modelled as adiabatic smooth no-slip walls. The IAPWS Library was used to define the material properties for the water with supercritical pressure in the case of heating.

The inferential effects of boundary conditions on the CFD results have not yet assessed. This question should be investigated in the next step of this work.

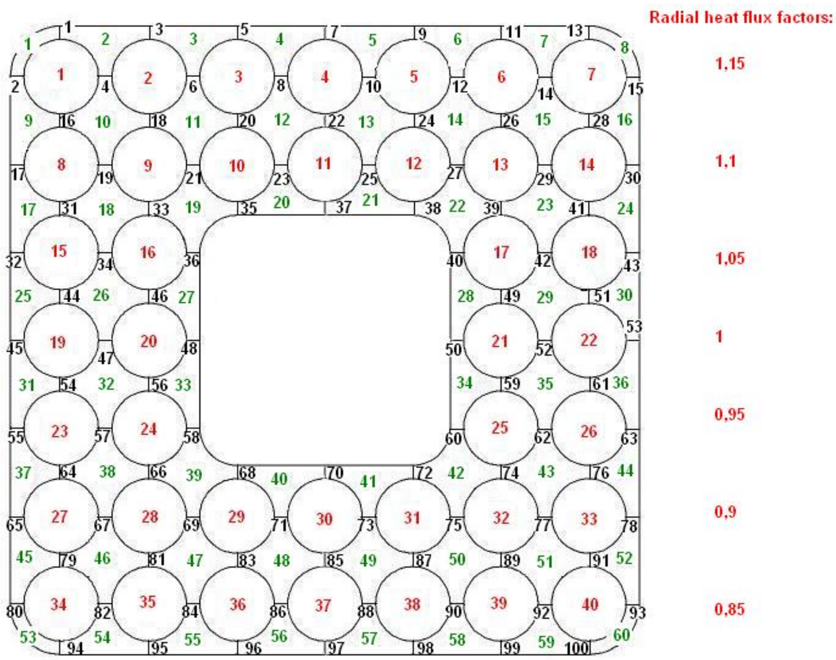

Figure 5. The numbering of sub-channels (green numbers), gaps (black numbers), fuel rods (red numbers) and the radial heat flux factors.

3. Some Details on Numerical Grid Generation and Computations

The aim of this investigation is to gain experience about CFD modelling of the whole perimeter HPLWR fuel assembly and to provide qualitative and quantitative insight about the inter-channel cross flow and mixing. Considering the high number of computational cases relatively coarse numerical meshes have been used to discretize the geometry. Fine boundary mesh is not applied to model suitably the near wall region. That is why the wall temperature and the near wall fields are not accurate enough to be investigated in detail. The scalable wall function has been used to model the near wall region. The geometry and mesh (with the automatic tetra meshing method) was created in the ANSYS ICEM CFD 11 SP1. The unstructured tetrahedral meshes of the cases differ only in the total number of nodes due to different global mesh size. Fig. 6 shows some details of the unstructured meshes.

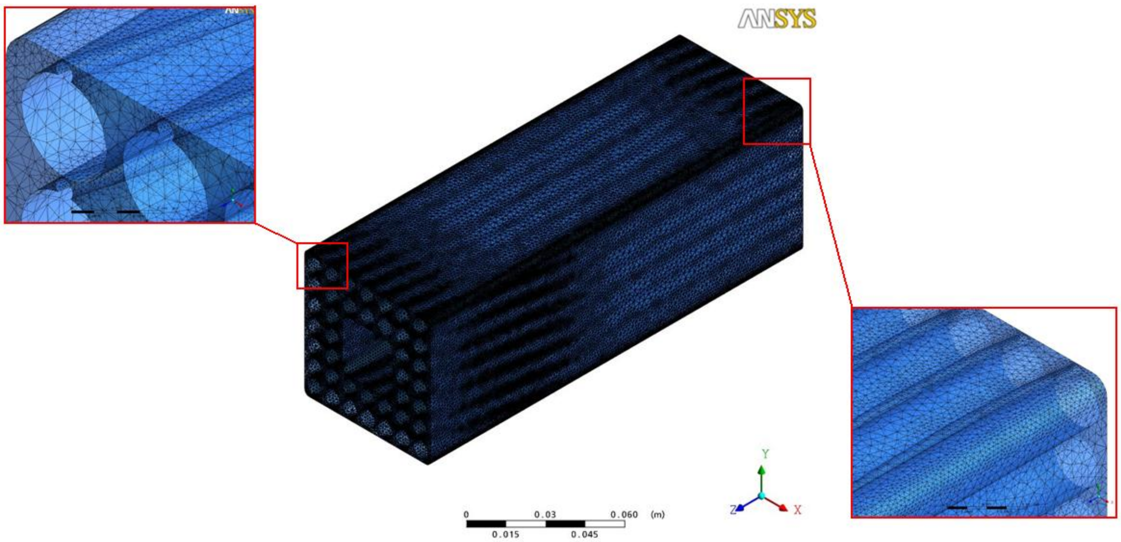

Figure 6. Some details of the unstructured tetrahedral mesh with 1,671,793 total number of nodes.

A big effort has been done to generate a structured or hybrid mesh to the above described complex geometry but these attempts have not been successful up to this day. The main meshing difficulties are the discretization of the wrapped wires and the 0.1 mm gap between wires and other walls (walls of fuel rods, fuel assembly box and moderator box). Finally, unstructured tetrahedral cells were used to discretize this fuel assembly part of HPLWR core.

All of the computations were performed on a NEC Xeon EM 64T type cluster named “cacau1” at HLRS (Peak Performance: 2.5 TFlops). Cacau1 has 200 dual nodes with 400 Intel Xeon EM64T CPU's (3.2GHz) for high performance computation. ANSYS CFX 11 SP1 and ICEM CFX 11 SP1 were used in parallel mode on cacau1 for the computations. Table II summarizes the used number of processors, wall clock times, maximum residual and imbalance values for each computational group. Many so called “User Points” were monitored during the calculations, for example: the area average of the pressure and velocity on the inflow and outflow regions, fluid temperature and velocity in many prescribed points, etc. The User Points and the imbalances indicated that all of the cases are well converged which means each value converged to a certain value (almost zero for imbalances) and does not changing with the iterations any more.

Table II. Characteristic computational data for each computational group.

Computational group	**Number of processors/iteration**	**Wall clock time**	**Max. RMS residual value**	**Max. imbalance value**	**Final/Peak RMS residual ratio**
HDR-G	16-32/500-1000	9-10h	$9\ 10^{-6}$	0.1844 %	10^{-4} - 10^{-5}
TH-G	16/200-300	10h-11h	10^{-7}	0.0395 %	10^{-5} - 10^{-6}

The convergence values are acceptable considering the proposal of the guidelines [11]:

- Not swirling flows are well converged with a reduction of only 3-4 orders of the final/peak RMS residual ratios.

- In case of swirling flow (which is valid for all cases presented here) 5-6 orders of the final/peak RMS residual ratios is necessary and acceptable for converged CFD calculation.

4. Mesh Sensitivity Study for Hydraulics and Thermal Hydraulics

Two target variables have been selected: the pressure drop along the model length for hydraulic calculations and the enthalpy rise between the inflow and outflow regions for thermal hydraulic cases. Table I indicates those cases which were used to investigate the mesh sensitivity for both computational groups. To demonstrate the mesh sensitivity the Richardson extrapolation has been applied. The value of an integral parameter (practically the target variable) of the flow should approach to a certain value if the mesh is finer and finer. This is an indicator for the accuracy and mesh suitability to discretize such geometry. Furthermore the Finite Volume Method is a secondary accurate method that is the reason for the reciprocal value of the square of the total number of nodes (1/N2) should be used as an independent variable for Richardson extrapolation (see Fig. 7 for hydraulic cases and Fig. 8 for thermal hydraulic cases).

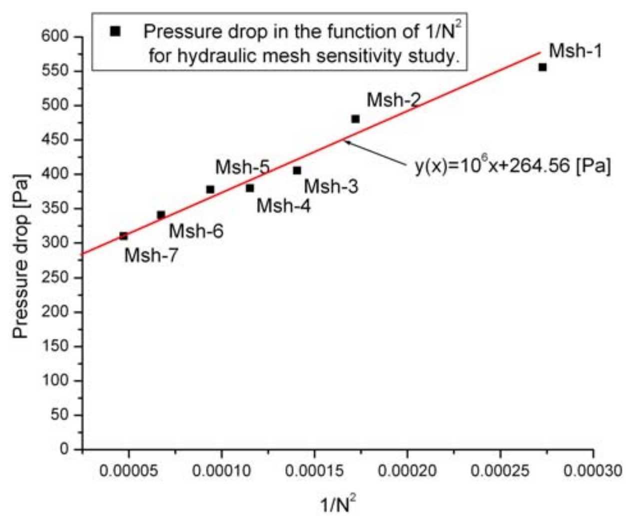

Figure 7. The pressure drop in the function of $1/N^2$ for the hydraulic mesh sensitivity study.

The pressure drop is monotonically decreasing if the number of nodes increases up to 265 Pa (perfect discretization see Fig. 7). After a detailed evaluation and comparison the size of Msh-6 has been selected for the thermal hydraulic cases. The enthalpy rise for the four thermal hydraulic cases shows identical result than the pressure drop before: monotonically increasing if the number of nodes increases up to 77.3 kJ/kg (perfect discretization see Fig. 8). Considering the data of Table II and the results of Fig. 7-8 the evaluated results presented in the next section are well established.

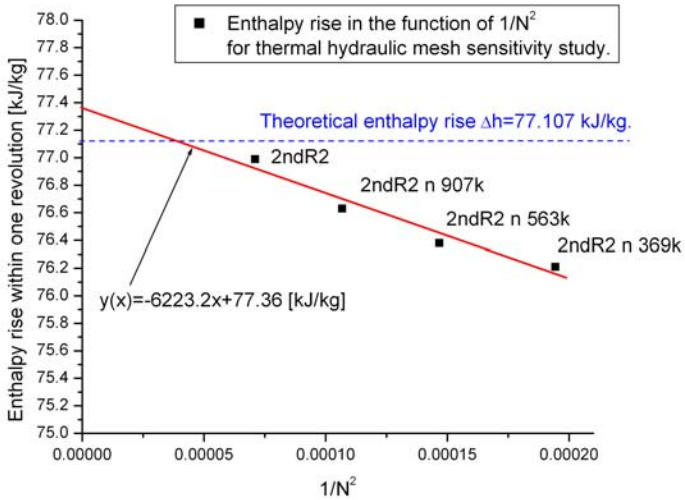

Figure 8. The enthalpy rise in the function of $1/N^2$ for the thermal hydraulic mesh sensitivity study.

5. Computational Results

This section is divided into three parts. In the first part the main characteristics of the flow pattern is introduced by hydraulic cases. In the second part the effect of heating on the inter-channel cross flow is investigated for reference hydraulic cases and heated cases with different heat flux profiles. In the last part the effect of heating on the swiping flow is assessed comparing reference hydraulic cases and heated cases with axial heat flux profiles.

5.1 The general characteristics of the flow pattern

The wrapped wire (as unusual spacer devices in HPLWR fuel assembly) causes an additional rotation component to the main axial flow velocity due to the flow strongly follow the wires. This type of flow is the so called swiping flow. The inter-channel cross flow far more influenced and enhanced by the presence of wrapped wires compared to the effect of anisotropic turbulence and different hydraulic diameters of the sub-channels proven by previous study [9,10]. The reason is that the geometry of the wires strongly guides the flow so the streamlines are swiped. Furthermore the hot spot in the outer corner sub-channels disappear due to the application of the wrapped wires discussed in another study [12].

Fig. 9 shows the locally scaled pressure fields of cross sections at 0 (inflow boundary region), 50, 100, 150, 200 (outflow boundary region) mm. As expected the pressure field rotate with the wires in a counter-clockwise direction.

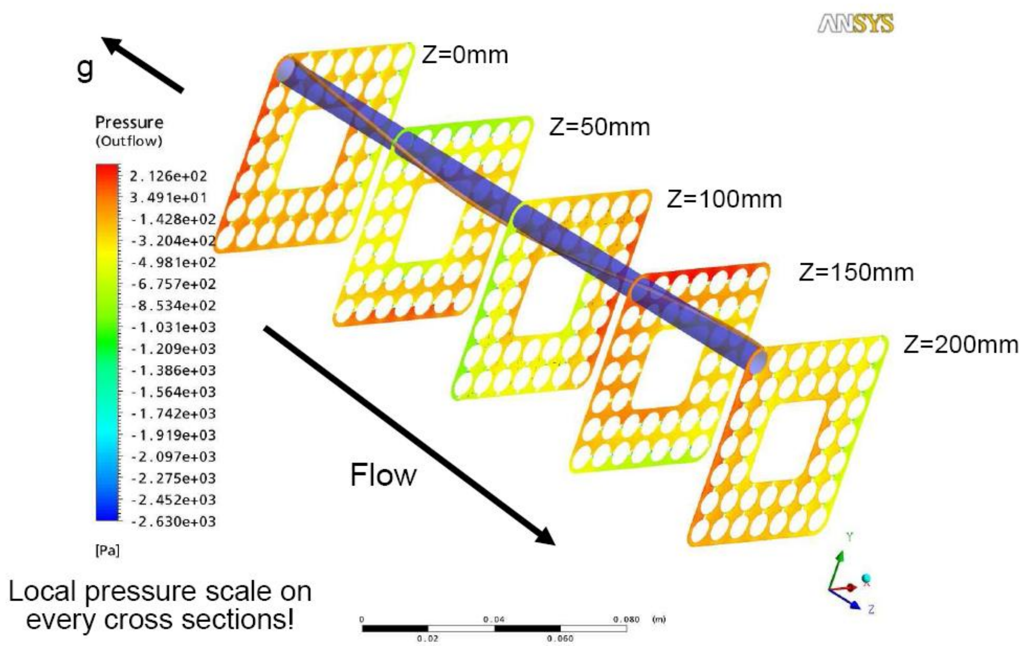

Figure 9. One fuel rod and wrapped wire and the locally scaled pressure fields of cross sections at 0, 50, 100, 150, 200 mm.

The counter-clockwise wire direction which included the HPLWR fuel assembly (see Fig. 2) leads to another characteristic features. The wires wrapped around such a fuel rod which is a neighbour to the fuel assembly wall crosses only once the gap between the fuel assembly wall and fuel rod and guide the flow always in counter-clockwise direction. This feature leads to a counter-clockwise inter-channel cross flow near the fuel assembly wall (see Fig. 10).

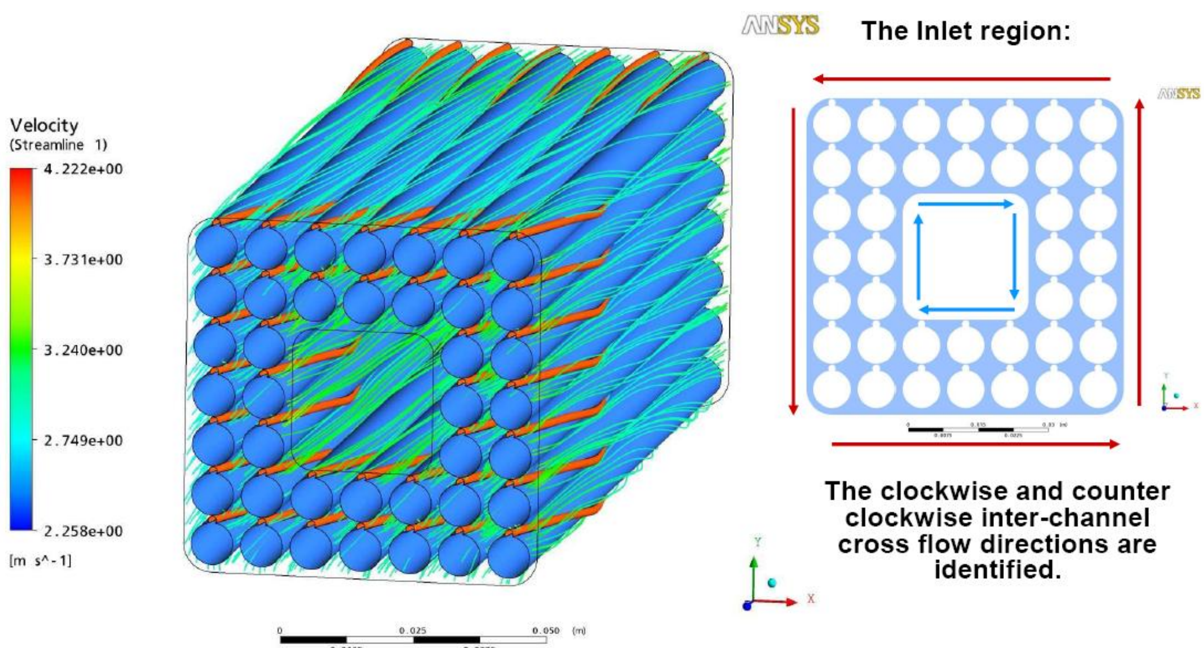

Figure 10. Streamlines originated from the inflow boundary region (left) and the recognized clockwise and counter-clockwise inter-channel cross flow directions.

The wires wrapped around such a fuel rod which is a neighbour to the moderator box wall crosses also only once the gap between the moderator box wall and fuel rod and guide the flow always in clockwise direction. This feature leads to a clockwise inter-channel cross flow near the moderator box wall (see also in Fig. 10). Two wires cross the gap in case of such a gap which is not located near the fuel assembly or the moderator box walls. It means that bidirectional inter-channel cross flow occurs at the "inner" (located between two fuel rods) gaps and unidirectional inter-channel cross flow occurs at the "outer" (located between a fuel rod and the fuel assembly or the moderator box walls) gaps.

5.2 The effect of heating on the inter-channel cross flow

There are four different sub-channel types in the square fuel assembly of HPLWR [13] as it can be seen in Figure 11. It is obvious that each gap is unique but anyway they should by classified somehow. To classify the gaps between the sub-channels the four sub-channel types are used. Based on the four sub-channel types six different gap types can be identified (see Table III and Figure 11).

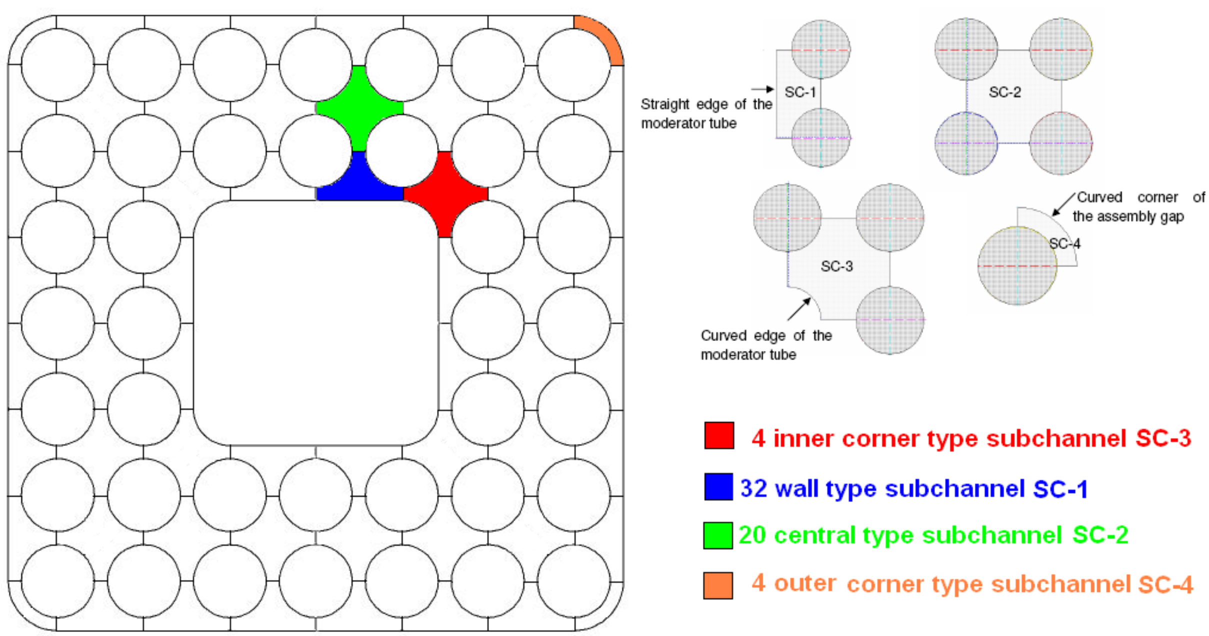

Figure 11. The four sub-channel types of the square fuel assembly of HPLWR [13].

Seven gaps (see in the last column in Table III) have been selected to represent the inter-channel cross flow for the six investigated gap types. These gaps are bounded by twelve sub-channels (SC No. 4, 5, 8, 14, 15, 16, 20, 21, 22, 23, 28, 29).

Table III. The types of the gaps defined by the four sub-channel types.

Name of gap type:	SC type at the first side:	SC type at the second side:	Number of representative Gaps:
Gap-I, wall-wall	SC-1, wall type	SC-1, wall type	7, 37
Gap-II, wall-central	SC-1, wall type	SC-2, central type	28
Gap-III, wall-inner	SC-1, wall type	SC-3, inner type	40
Gap-IV, wall-outer	SC-1, wall type	SC-4, outer type	15
Gap-V, inner-central	SC-3, inner type	SC-2, central type	27
Gap-VI, central-central	SC-2, central type	SC-2, central type	42

Fig. 12 shows a comparison between the mass flow averaged lateral velocity of hydraulic (1stR, 2ndR, 3rdR) and thermal hydraulic (1stR1, 2ndR1, 3rdR1) cases using Gap-7 and 15. Sixteen so called "User surface" (CFX terminology) have been used to each gap to evaluate the mass flow averaged lateral velocities on them. The average difference between 1stR and 1stR1 of Gap-7 and 15 are 9.7% and 1.51%. The average difference between 2ndR and 2ndR1 of Gap-7 and 15 are 13.5% and 6%. The average difference between 3rdR and 3rdR1 of Gap-7 and 15 are 8.95% and 1.45%.

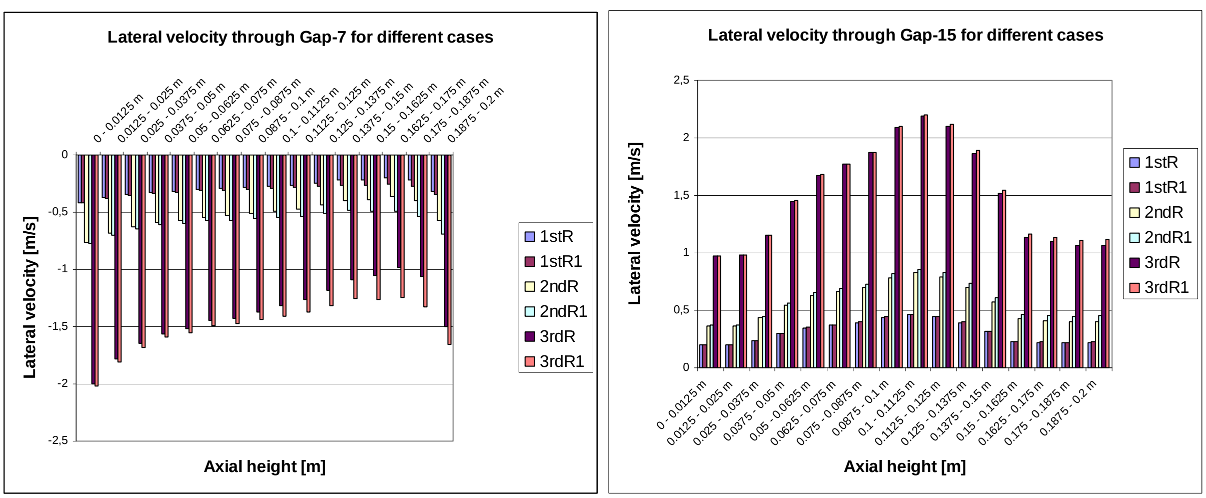

Figure 12. Comparison between the mass flow averaged lateral velocity of hydraulic and thermal hydraulic cases using Gap-7 (left) and 15 (right).

Fig. 13 shows a comparison between the mass flow averaged lateral velocity of differently heated thermal hydraulic cases (axial, constant and axial heat flux distribution with radial heat flux factors) using Gap-27. The first and last one-fourth part of the gap show positive and the second-third one-fourth show negative lateral velocity due to two wires cross Gap-27 at the position of one-fourth and three-fourth. The lateral velocity of Gap-27 in the first one-fourth part is positive due to the cross flow is affected by the wire of fuel rod No. 12 in the previous revolution. At the position of one-fourth the wire of fuel rod No. 13 crosses Gap-27 and change the cross flow direction from positive to negative. The negative cross flow direction is valid up to the position of three-fourth where the wire of fuel rod No. 12 change this direction from negative to positive (see Fig. 13).

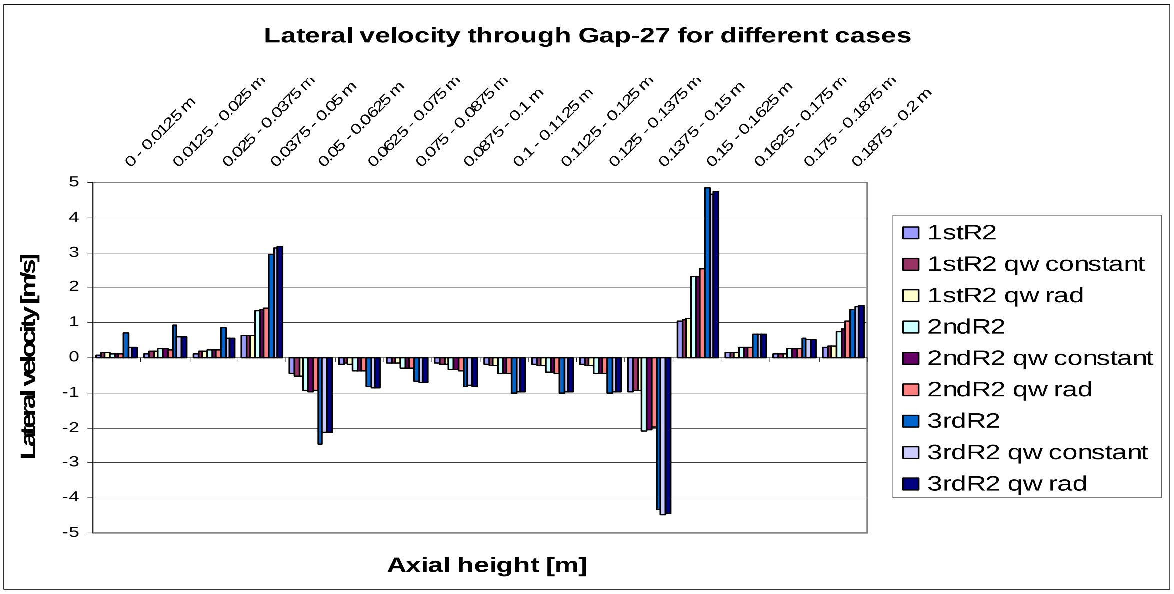

Figure 13. Comparison between the mass flow averaged lateral velocities of differently heated thermal hydraulic cases.

The average difference between 1stR2 and 1stR2 qw constant of Gap-27 is 13.23%. The average difference between 1stR2 qw constant and 1stR2 qw rad of Gap-27 is 13.57%. The average difference between 2ndR2 and 2ndR2 qw constant of Gap-27 is 0.56%. The average difference between 2ndR2 qw constant and 2ndR2 qw rad of Gap-27 is 2.16%. The average difference between 3rdR2 and 3rdR2 qw constant of Gap-27 is 6.7%. The average difference between 3rdR2 qw constant and 3rdR2 qw rad of Gap-27 is 7.13%.

Fig. 14 shows a comparison between the mass flow averaged lateral velocities of the thermal hydraulic cases in three following revolutions using Gap-27. The average difference between 1stR1 and 1stR2 of Gap-27 is 7.38%. The average difference between 1stR2 and 1stR3 of Gap-27 is 0.19%. The average difference between 2ndR1 and 2ndR2 of Gap-27 is 4.77%. The average difference between 2ndR2 and 2ndR3 of Gap-27 is 0.29%. The average difference between 3rdR1 and 3rdR2 of Gap-27 is 1.36%. The average difference between 3rdR2 and 3rdR3 of Gap-27 is 6.69%.

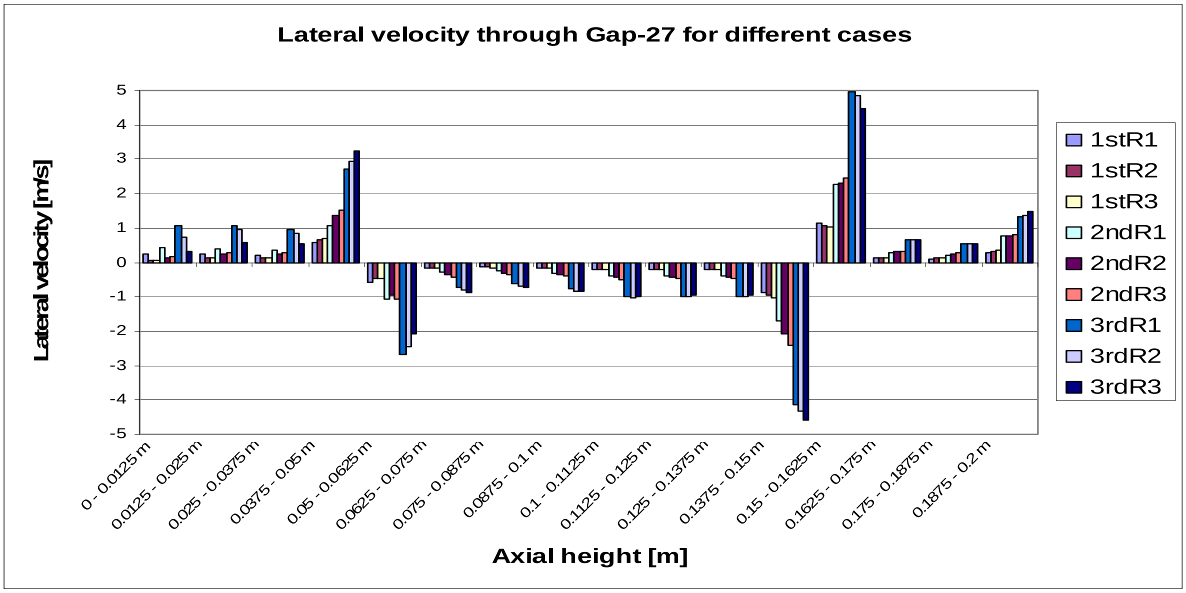

Figure 14. Comparison between the mass flow averaged lateral velocities of the thermal hydraulic cases in three following revolutions.

Fig. 15 shows the comparison between the mass flow averaged lateral velocities of the 1stR2 case for the seven representation gaps (see Table III).

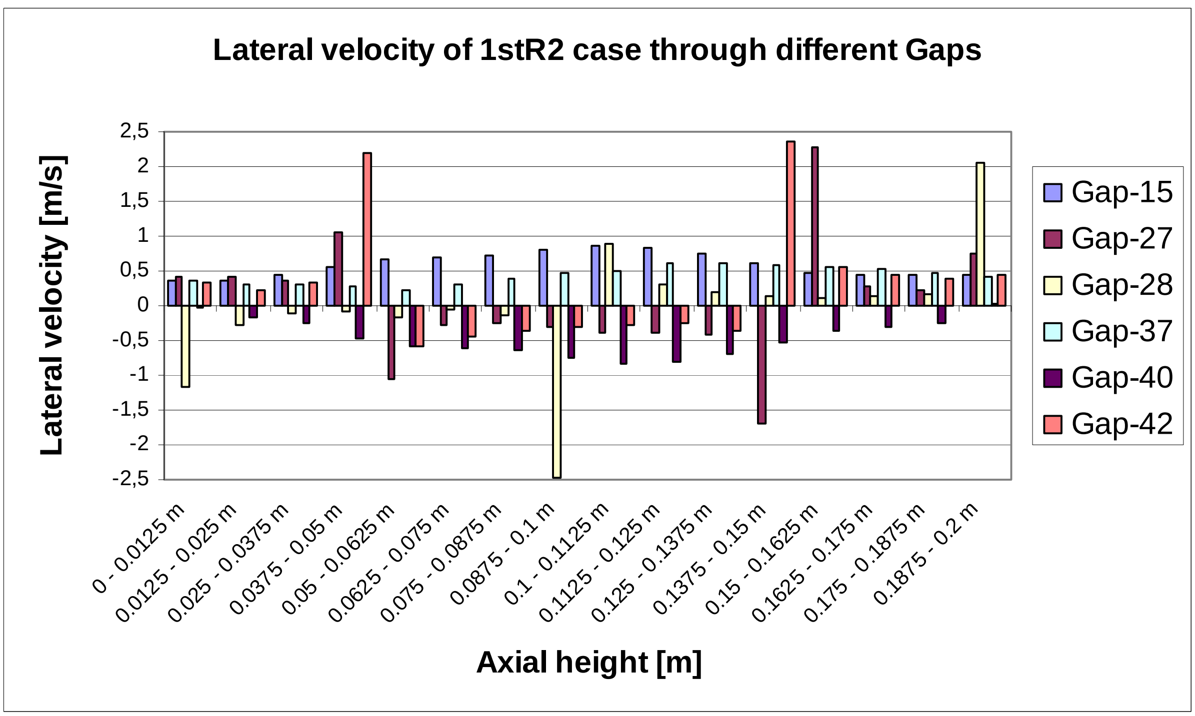

Figure 15. Comparison between the mass flow averaged lateral velocities of the 1stR2 case for the six representation gaps.

The spatial discretization was finer in the region where the solid walls were close to each other (where wires cross gaps) but these finer mesh zones seems to be not suitably dense enough. The velocity gradients are large here and the lateral velocities go from positive or negative values to negative or positive values. That is the reason for some unrealistic velocity values are expected at such a zone where the lateral velocities change their directions: relatively high lateral velocities can be seen for Gap-27, 28, 42 around 50 mm and 150 mm, 100 mm, 50 mm and 150 mm respectively, see Fig. 15. In the further research this problem should be solved with finer numerical meshes in the vicinity of close solid walls.

5.3 The effect of heating on the sweeping flow

Fig. 12 and 16 show comparison between mass flow averaged lateral velocity of hydraulic and thermal hydraulic cases using Gap-7 and 15 (outer swiping cycle) and Gap-37 and 40 (inner swiping cycle). The heating has a slight effect on the swiping flow and its quantitative degree is under investigation.

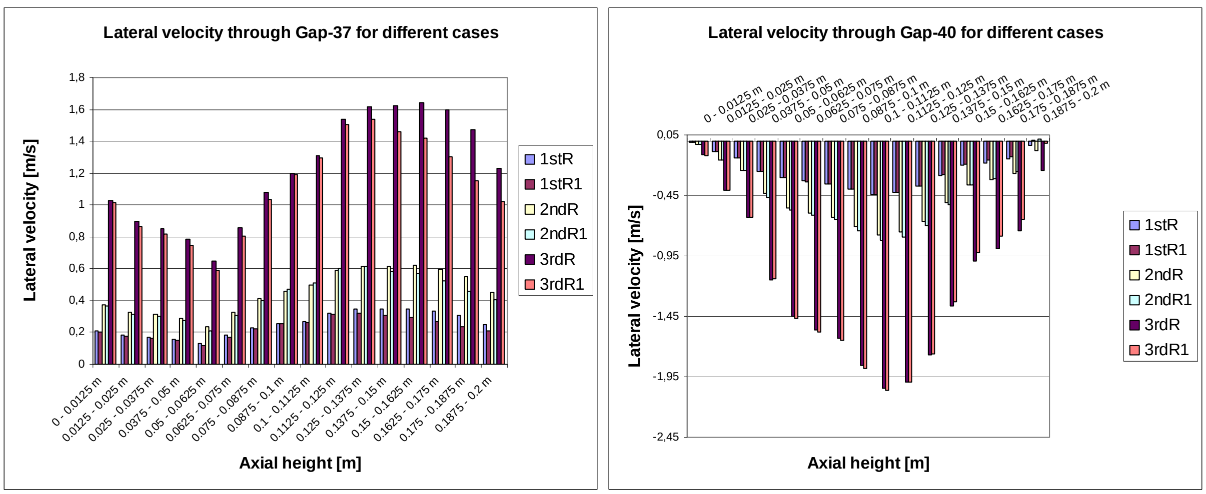

Figure 16. Comparison between the mass flow averaged lateral velocity of hydraulic and thermal hydraulic cases using Gap-37 (left) and 40 (right).

6. Conclusion

The present paper demonstrates, that with consequent numerical effort a reasonable result of CFD calculation on a part of HPLWR fuel assembly can be achieved using unstructured tetrahedral grids, the Reynolds-stress turbulence model and a combination of cases with hydraulic and thermo hydraulic boundary conditions. The expected flow properties such as additional mixing and the sweeping flow are qualitatively reproduced as expected. A quantitative comparison to the results of a sub-channel code has now become possible in order to better understand and possibly improve the sub-channel models for wrapped-wire geometries. The authors are aware of the limitation of the results shown above. Validation of the present results to measured data of proper experiments is still needed.

7. Acknowledgement

This work is connected to the scientific program of the " Development of quality-oriented and harmonized R+D+I strategy and functional model at BME" project. This project is supported by the New Hungary Development Plan (Project ID: TÁMOP-4.2.1/B-09/1/KMR-2010-0002).

8. References

[1] K. Fischer, T. Schulenberg, and E. Laurien, "Design of a supercritical water-cooled reactor with a three-pass core arrangement," Nuclear Engineering and Design, Vol. 239, Iss. 4, 2009, pp. 800-812.

[2] T. Schulenberg et al., "European supercritical water cooled reactor," Proceedings of FISA, Prague, Czech Republic, 2009 June 22-24.

[3] H. Li, H. Wang, Y. Luo, H. Gu, X. Shi, T Chen, E. Laurien, and Y. Zhu, "Experimental investigation on heat transfer from a heated rod with a helically wrapped wire inside a square vertical channel to water at supercritical pressures," Nuclear Engineering and Design, Vol. 239, Iss. 10, October 2009, pp. 2004-2012.

[4] S. Himmel, A.G. Class, E. Laurien, T. Schulenberg, "Determination of Mixing coefficients in a wire-wrapped HPLWR fuel assembly using CFD," in: Proceedings of ICAPP-08, Anaheim, CA, USA, 2008 June, paper 8053.

[5] L. Monti, J. Starflinger, and T. Schulenberg, "Effectiveness of an insulated fuel assembly to improve HPLWR core performance," Proceedings of 4th Int. Symp. on Supercritical Water-Cooled Reactors, Heidelberg, Germany, 2009 March 8-11.

[6] R. Gajapathy, K. Velusamy, P. Selvaraj, P. Chellapandi, and S.C. Chetal, "CFD investigation of helical wire-wrapped 7-pin fuel bundle and the challenges in modeling full scale 217 pin bundle," Nuclear Engineering and Design Vol. 237, Iss. 24, 2007, 2332-2342.

[7] P. Fischer, J. Lottes, A. Siegel, and G. Palmiotti, "Large Eddy Simulation of wire-wrapped fuel Pin-I: Hydrodynamics in a periodic array," Proc. of Joint Int. topical Meeting on Mathematics & Computation and Supercomputing in Nuclear Applications (M&C+SNA 2007), Monterey, California, 2007 April 15-19.

[8] U. Bieder, F. Ducros, G. Fauchet, and P. Quembere, "CFD investigation of a full scale helical wire-wrapped 61-pin fuel bundle by using the code TRIO_U," Proceedings of Annual Meeting on Nuclear Technology, Dresden, Germany, 2009 May 12-14.

[9] A. Kiss, E. Laurien and A. Aszódi, "Numerical Simulation of a HPLWR Fuel Assembly Flow With Wrapped Wire Spacers," Proceedings of ICAPP 2008 Conference (Paper 8339), Anaheim, California, USA, 2008, June 9-12.

[10] E. Laurien, T. Wintterle, "On the Numerical Simulation of Flow and Heat Transfer within the Fuel-Assembly of the High-Performance Light-Water Reactor," Proceedings of KTH-Workshop on Modeling and Measurements of Two-Phase Flows and Heat Transfer in Nuclear Fuel Assemblies, Stockholm, Sweden, 2006 October 10-11.

[11] F. Menter et al. „CFD Best Practice Guidelines for CFD Code Validation for Reactor-Safety Applications," ECORA project, FIKS-CT-2001-00154, Brussels, Belgium (2002).

[12] E. Laurien, T. Wintterle, "Secondary Flows in the Cooling Channels of the High-Performance Light-Water Reactor," Proceedings of ICAPP 2007 Conference (Paper 7089), Nice, France, 2007 May 13-18.

[13] C. L. Waata, "Coupled Neutronics / Thermal-hydraulics Analysis of a High-Performance Light-Water Reactor Fuel Assembly," doctoral thesis, FZKA 7233, July, 2006.